Scalable Computing: Practice and Experience, ISSN 1895-1767, http://www.scpe.org
© 2024 SCPE. Volume 25, Issues 6, pp. 5021–5038, DOI 10.12694/scpe.v25i6.3425

PE GAS PIPELINE DEFECT DETECTION ALGORITHM BASED ON IMPROVED YOLO V5

QIANKUN FU*, QIANG LI †, WENSHEN RAN ‡, YANG WANG §, NAN LIN ¶, AND HUIQING LAN ‖

Abstract. In order to improve defects detection efficiency in polyethylene (PE) gas pipelines and decrease leakage or other pipelines abnormalities in operation, this research proposed an improved YOLO(You Only Look Once) v5 detection model. First, the collected pipeline defect images were processed in grey scale, which improved the computational efficiency of the computer; then, Gamma transform and double filtering algorithms were applied respectively for image enhancement and noise reduction filtering of defects, which enhanced image quality and reduced image noise. Finally, the improved Sobel algorithm was applied to detect defective image edges and the defects in the image were segmented by adaptive threshold segmentation method to obtain binary images. The obtained binary images were employed to train the improved YOLO v5 detection model. The obtained experimental results showed that, compared with the original algorithm, the improved detection algorithm had better detection efficiency and higher robustness as well as higher recognition for common defects,improved YOLOv5 mAP and recall were 97.18% and 98.03%, respectively, the mAP has increased by 1.33% and the recall has increased by 3.83%,which can achieve the detection and identification of defect types of effects in PE gas pipes.

Key words: Defect detection; Image processing; Machine learning; YOLO v5; Attention mechanism

1. Introduction. Today, PE pipelines are widely being used as an economical and effective transportation means for oil, gas and urban water heating supply, which brings much convenience to human life as well as industrial and agricultural development and also produces great economic benefits [1]. This type of pipeline transportation has been used since 1860s, when the world's first crude oil pipeline was constructed in the state of Pennsylvania in the United States [2]. Today, after decades of development, pipeline transport industry has become the fifth largest means of transport after railways, roads, aviation and seaborne [3]. However, PE oil and gas pipelines are buried deep in the ground and are vulnerable to corrosion, cracks and other damage types in long-term in the presence of oil or gas and other substances [4]. In pipeline networks around the world, cracks and other damage forms in pipelines can lead to the leakage of liquids and gases, resulting in wasted resources, environmental pollution, and even explosions [5]. Due to the long time required for manual inspection of pipelines, pipeline robotics equipped with various inspection methods have been developed and applied [6]. Robots equipped with image recognition technology has become an increasingly popular method for online non-contact inspection in recent years. By utilizing image recognition technology for inspection, it is possible to clearly identify existing defects [7].

As time passed, image processing technology has rapidly come into prominence and at the same time, pipeline defect detection technology has also presented a diversified trend [8]. Dong et al. [9] developed an automatic pipeline weld defect identification technology applicable of quality identification and assessment of a series of defects in pipeline welds, with an identification accuracy rates of higher than 90%, which helped ensure the safe operation of pipelines. Wang et al. [10] introduced a framework for tracking multiple sewer defects in CCTV videos based on defect detection and metric learning. This fast method enabled high-accuracy detection of general 2D surface defects. Bondada et al. [11] presents a new method for automated inspection

*School of Mechanical Engineering, Xinjiang University, Urumqi, Xinjiang 830046, China
†Xinjiang Uygur Autonomous Region Inspection Institute of Special Equipment, Urumqi 830000, China.
‡Pressure Pipe Department, China Special Equipment Inspection and Research Institute, Beijing 100013, China.
§School of Mechanical Engineering, Xinjiang University, Urumqi, Xinjiang 830046, China (Corresponding author, ywangxju@xju.edu.cn)
¶Pressure Pipe Department, China Special Equipment Inspection and Research Institute, Beijing 100013, China.
‖Laboratory of Vehicle Advanced Manufacturing, Measuring and Control Technology (Ministry of Education), Beijing 100044, China.

Fig. 2.1: Image pre-processing procedure.

of long distance pipelines using machine vision technology. The method identifies corrosion and quantifies the damage caused to help maintain pipeline integrity. Myrans et al. [12] developed a new method for automatic identification of detected fault types in pipelines. Their proposed method computed GIST feature descriptors for fault frames and applied RF machine learning classifiers to analyze frame contents and identify fault types. Ye et al. [13] introduced an image recognition algorithm using feature extraction and machine learning methods and applied support vector machines to classify pipeline defects with 84.1% overall accuracy. Fang et al. [14] developed a fault detection technique that applied an anomaly detection algorithm developed using unsupervised machine learning to a new pipeline visual inspection device. The video recorded by the device was regarded as a sequence signal, which was converted into a feature vector and then, defects were identified using a pipeline defect detection algorithm. The overall accuracy of the developed method was above 90%. Kumar et al. [15] developed a framework that used a deep convolutional neural network (CNN) to classify multiple defects such as root intrusion, deposits, and cracks in sewer closed circuit television (CCTV) images.

YOLO algorithm is also gradually becoming popular in pipeline defect detection thanks to the development of deep learning. Chen et al. [16] developed a Cycle-GAN-based sample enhancement strategy and an improved YOLO v5-based defect detection system for the detection of pipeline inner wall defects, which could detect common problems including oxide spalling, erosion, deposition, and infiltration. Zhao et al. [17] proposes a YOLOv3-based method for underwater pipeline oil spill point detection. Their developed network was able to quickly detect pipeline leakage points with high accuracy and low misdetection rate. Yan et al. [18] introduced an anomalous signal detection method (YOLO-PD) based on improved YOLOv7 which was able to effectively identify anomalous signals in pipelines with higher detection accuracy. Peng et al. [19] improved YOLO v5 algorithm and introduced an algorithm for pipeline leakage detection using CBAM(Convolutional block attention module) attention mechanism, thereby focusing more on identifying pipeline leakage characteristics and decreasing intricate background effects on detection outcomes. Yin et al. [20] developed a YOLO v3-based pipeline defect detection framework capable of detecting six common pipeline defects with mean average precision (mAP) of 85.37%.

In summary, the above mentioned computer vision-based inspection methods were consisted of three parts; namely, image preprocessing, feature extraction, and defect identification and classification. These methods were more effective in detection and required less labor. However, many current feature extraction methods are designed for specific defect types and can only recognize them, which limits their applicability. Furthermore, they suffer from low precision and high incorrect detection rate. Hence, this research developed a YOLOv5-based PE pipeline defect detection framework capable of extracting abstract features of defects on its own and accurately detecting and categorizing three types of defect; namely cracks, snaps, and holes. Accordingly, this research improved the existing modeling frameworks by adding an attention mechanism model and K-means++ algorithm and employed ablation experiments to validate the efficiency of the developed mod-el. It was found that unlike the original algorithm, mAP was increased by 1.33% and maximum confidence was enhanced by 0.2

2. Image Pre-processing. Pipe image pre-processing not only eliminates noise, but also improves distinction between pipeline backdrop and defects, decrease data complexity and highlight defect characteristics [21]. The image pre-processing approach employed in this research is illustrated Fig. 2.1.

2.1. Greyscale processing for pipeline images. Greyscale is the brightness value of each pixel in an image and is often applied to represent the darkness or lightness of a pixel. Grayscale images are usually easier to process compared to color images since they have only one channel while color images have three channels [22]. Compared to colored images, grayscale images use less memory and more swiftly perform computer tasks.

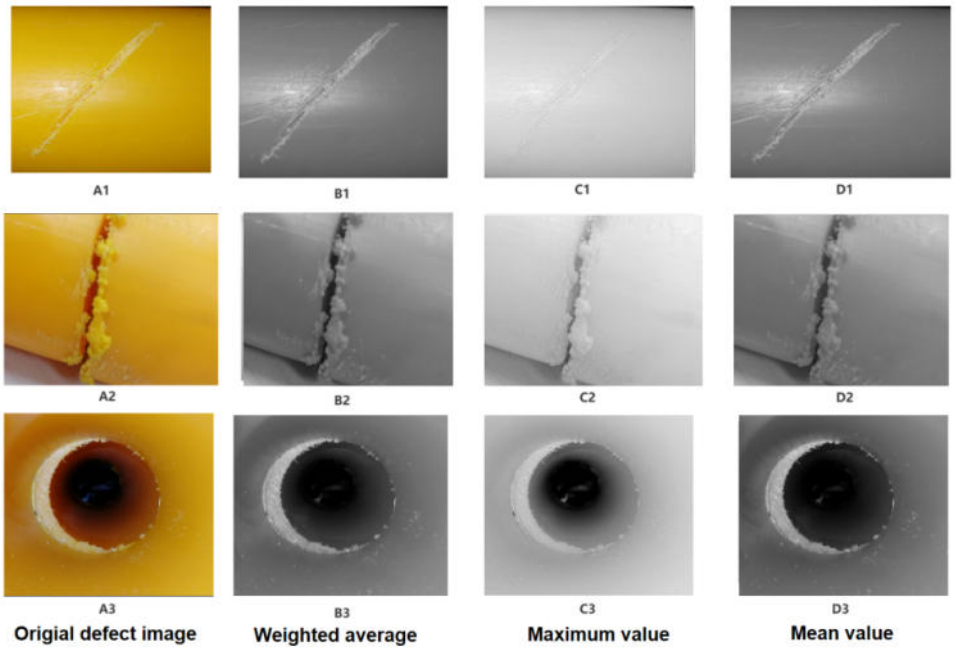

Fig. 2.2: Comparison of different greyscale processing methods.

The three prevalent methods to convert color images into grayscale ones are mean value, maximum value, and weighted average methods.

Maximum value method directly selects the highest-valued element from the color channels in images are red (R), green (G), and blue (B) as shown in equation(2.1).

$$R = G = B = \max(R, G, B) \tag{2.1}$$

Mean value approach averages the values in the three R, B, and G components. as stated in equation (2.2).

$$R = G = B = (R + G + B)/3 \tag{2.2}$$

Weighted average method relies on the sensitivity of human eye to the three colors R, B, G, as given in equation(2.3):

$$I(u, v) = 0.3 \times I_R(u, v) + 0.59 \times I_G(u, v) + 0.11 \times I_B(u, v) \tag{2.3}$$

Where: $I(u, v)$ indicates the coordinate's gray value, while $I_R(u, v)I_B(u, v)$ and $I_G(u, v)$ are pixel brightness levels for the three color elements of R, B and G, respectively.

Utilizing weighted average (Fig. 2.2B1-B3),maximum value (Fig. 2.2C1-C3) and mean value (Fig. 2.2D1-D3)techniques, the three initial defect image (Fig. 2.2 A1-A3) of holes,cracks, and snaps were processed in grayscale. It was found that weighted aver-age method was the most efficient technique for grayscale images. according to Fig. 2.2, pipeline defect image displays clear defect features and moderate brightness. Therefore, weighted average method was used for image grayscale in this research.

2.2. Enhancing images for pipeline defects. Enhancing the visual appeal of an image entails emphasizing its borders and key textural features, while minimizing the visibility of less significant sections, thereby slightly boosting image visual impact [23]. To improve grayscale image (Fig. 2.3A1-A3), Gamma transformation (Fig. 2.3B1-B3), global histogram equalization (Fig. 2.3C1-C3), and adaptive histogram equalization (Fig. 2.3D1-D3) were applied.

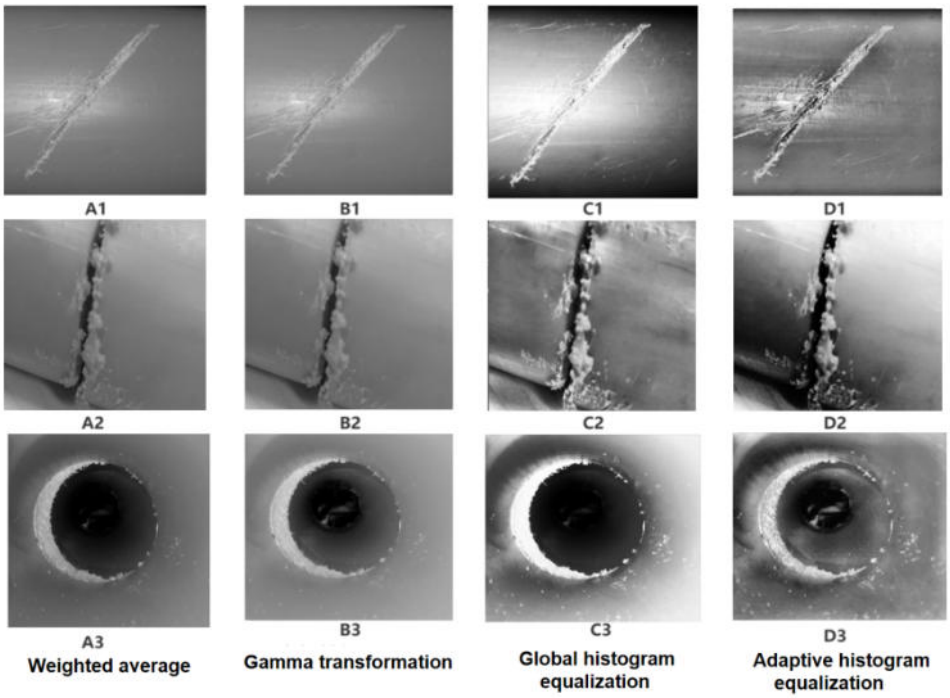

Fig. 2.3: Comparison of the effectiveness of different image enhancement algorithms.

It was seen from Fig. 2.3 that, compared to other algorithms, Gamma transformation created no distortion in pipe defect images and defect borders became more visible and prominent in the backdrop. Therefore, Gamma transform was applied to enhance contrast between pipeline backdrop and pipeline defects.

2.3. Filtering and denoising images of pipe defects. Due to environmental interference or equipment limitations, the final image is frequently susceptible to significant noise interference during image transmission process. Image denoising is a classic image restoration method which employs noise to predict clean images [24]. The above images (Fig. 2.4A1-A3) were denoised using bilateral filtering (Fig. 2.4C1-C3), Gaussian filtering (Fig. 2.4D1-D3), mean filtering (Fig. 2.4E1-E3) and median filtering (Fig. 2.4F1-F3).

Step-by-step processing is a popular approach for resolving complex noisy images [25]. A specific weighted average used in bilateral filtering employs Gaussian distribution to eliminate Gaussian noise from the image. However, elimination of Gaussian noise ignores salt-and-pepper noise and while adaptive median filtering excels at removing salt-and-pepper noise, its effectiveness falls when eliminating Gaussian noise[26]. There-fore, it was recommended to apply a dual filter (Fig. 2.4B1-B3), in which a median filter eliminated salt-and-pepper noise and then, a bilateral filter eliminated Gaussian noise. Unlike alternative filtering methods, dual filtering maintained edge details, removed noise points, and effectively preserved edges, as illustrated in Fig. 2.4 Consequently, this re-search utilized dual-filter noise reduction technique.

2.4. Edge detection of pipe defect image. Edge detection in images can help us better understand image contents, extract feature information, and achieve object detection and recognition.The traditional Sobel operator performs a weighted averaging operation on each pixel by applying a convolutional template (as illustrated in Fig. 2.5), followed by a differential procedure to obtain gradient values along X and Y directions. This algorithm cannot easily obtain the required detection outcomes and its localization precision falls short. Since the traditional Sobel algorithm has templates only along X (horizontal) and Y (vertical) directions, it is more sensitive to detect x and y edges [27]. The obtained PE gas pipe defect images included a high quantity of interfering data due to image compression and working environment and different forms and depths of defects

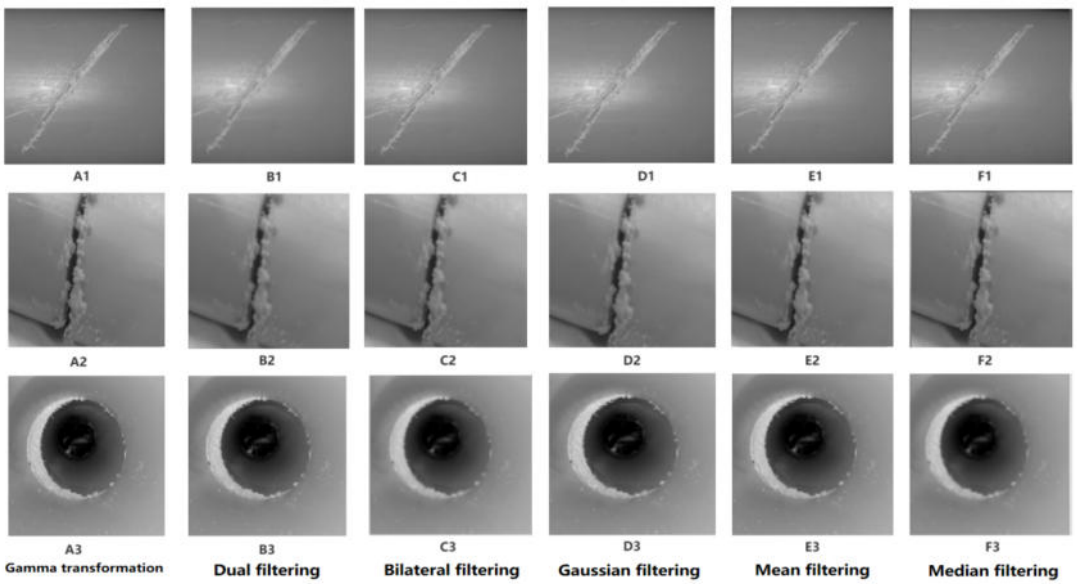

Fig. 2.4: Comparison of different image filtering algorithms.

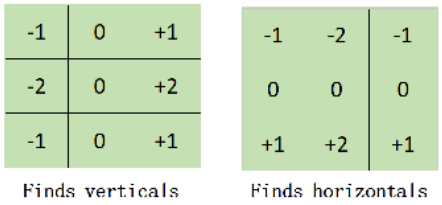

Fig. 2.5: Sobel operator template.

in the pipeline produced relatively tiny regional variations in defect image gray scale. Therefore, relying only on two directional operators for pipe defect edge detection was found to be inefficient and prone to missing edge information. Hence, it was proposed to add six more directions to traditional Sobel algorithm to enhance image edge pixel detection precision[28]. As illustrated in Fig. 2.6, this method enhanced image edge detection, boosted edge detection precision, and reduced erroneous edge chances.

On the above-displayed pipeline defect-filtered images (Fig. 2.7A1-A3), Sobel edge detection method (Fig. 2.7B1-B3), Prewitt edge detection method (Fig. 2.7C1-C3), and improved Sobel edge detection method (Fig. 2.7D1-D3) were applied for image border detection. Edge detection results of the three defects are illustrated in Fig. 2.7. In terms of result comparison, improved Sobel algorithm enhanced defect edge extraction, ensuring greater continuity and integrity, and fully revealed defect shape characteristics. Therefore, this research employed improved Sobel algorithm to identify edges.

2.5. Adaptive Threshold Segmentation. When faced with non-uniform lighting or irregular gray value distribution, the segmentation outcomes obtained with a global threshold are frequently unsatisfactory, whereas application of an adaptive threshold, also known as local segmentation, could provide favorable results [29]. The function of this concept was to determine local threshold based on the brightness distributions of various image regions rather than global image threshold. This allowed it to adaptively determine thresholds for various image regions; hence, it was called "adaptive thresholding method". Following edge detection, images (Fig. 2.8A1-A3) were processed through global threshold segmentation (Fig. 2.8B1-B3), Otsu threshold segmentation (Fig.

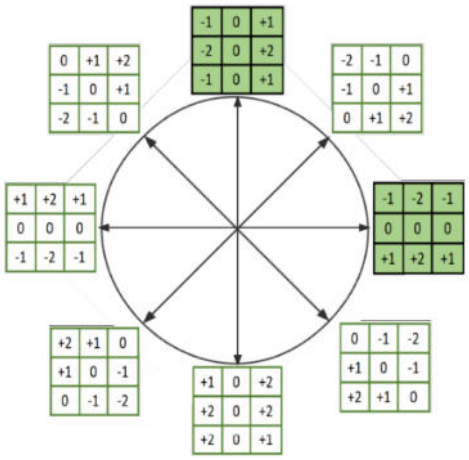

Fig. 2.6: Improved Sobel operator.

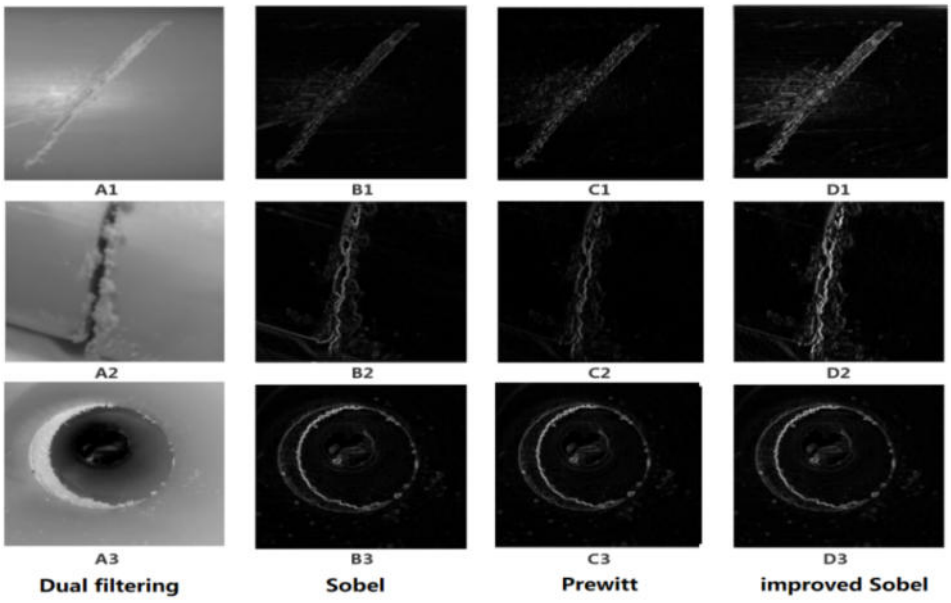

Fig. 2.7: Comparison of the effectiveness of different edge detection algorithms.

2.8C1-C3), and adaptive threshold segmentation (Fig. 2.8D1-D3). Through naked eye observation and using adaptive threshold pipe defects and backdrop could be distinguished to achieve optimal segmentation of PE gas pipe defects with minimal information interference. Therefore, in this research, adaptive threshold algorithm was applied for image division to obtain binary image.

3. Pipeline defect detection algorithm based on improved YOLOv5. YOLO v5 is part of You Only Look Once (YOLO) algorithm family. This algorithm has made some improvements on YOLO v4 and its speed and accuracy have been greatly improved [30]. The main idea of the algorithm was to use a single neural network model for target detection, by feeding the entire image into the model. The model was able to directly output the location and class information of the targets present in the image [31]. Three modules,

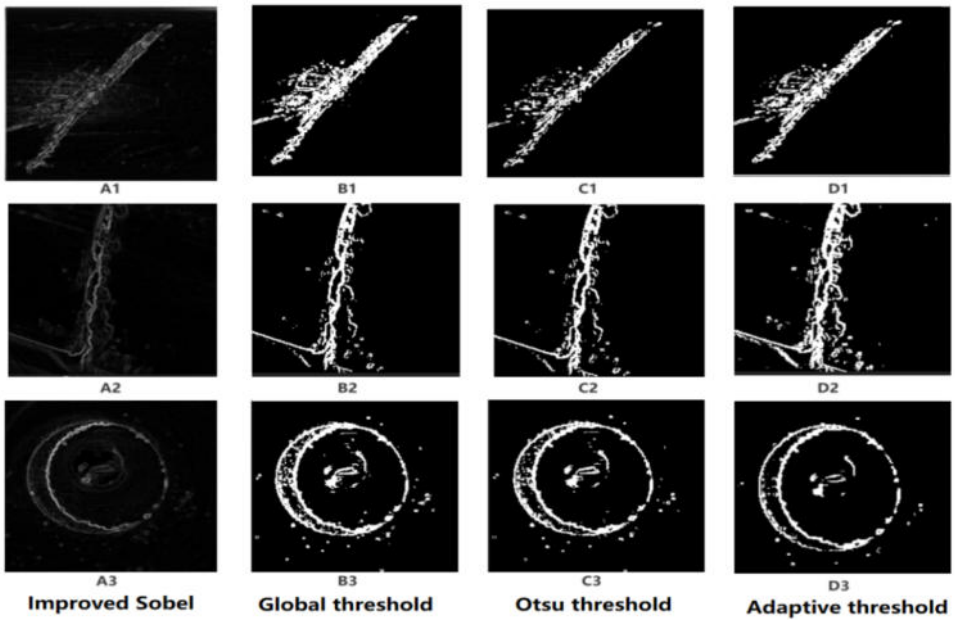

Fig. 2.8: Comparison of different threshold segmentation methods.

Fig. 3.1: Conv module structure.

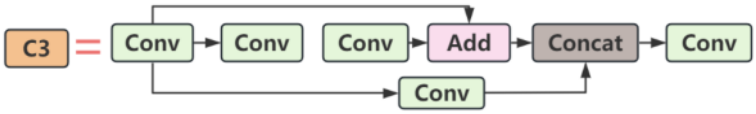

Fig. 3.2: C3 module structure.

namely backbone, neck, and head, make up YOLO v5 and use grids concept to detect targets.

3.1. YOLO v5 algorithm principle.

3.1.1. Backbone. Backbone is an image feature extraction network that takes input images and gradually extracts features through several convolutional and pooling layers [32]. The main structures of backbone are Conv module, C3 module, and SPP module, which play key roles in target detection algorithms.

1. Conv module. Convolutional neural networks frequently use conv module as fundamental module, which is mainly composed of Conv2d, BN layer and SILU activation function. High-level image features can be gradually extracted through these operations, which helps the network to learn various patterns and features in image and provide the necessary information for target detection. Conv module structure is illustrated in Fig. 3.1.

2. C3 module. C3 module can extract multi-scale feature information from receptive fields of various sizes. This is significant for computer vision applications such as target detection because it achieves higher accuracy and speed in shorter training times; therefore, it is extensively applied in target detection tasks. C3 module structure is illustrated in Fig. 3.2.

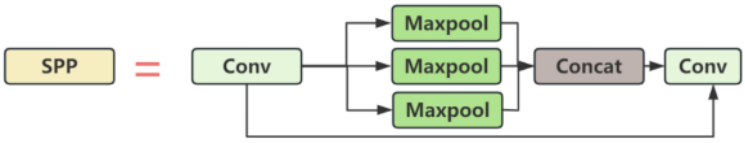

Fig. 3.3: SPP module structure.

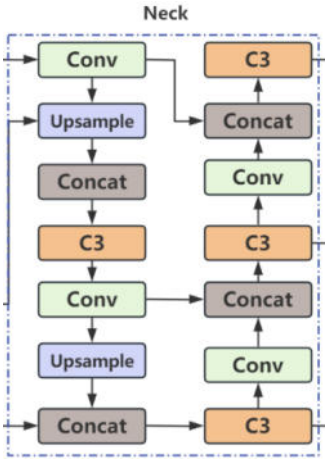

Fig. 3.4: Neck module structure.

3. SPP module. The role of spatial pyramid pooling (SPP) module is to perform multi-scale pooling operations on input feature maps to capture spatial information of different sizes. This helps the network better understand the contextual information of the target at different scales, improving target detection accuracy and robustness. The SPP module plays a key role in YOLO v5, helping the network to efficiently concatenate target features at different scales and improve detection performance. The structure of SPP module is illustrated in Fig. 3.3.

3.1.2. Neck module. Because the uncertainty of the size and position of an object in an image, a mechanism is required to handle targets of different scales and sizes. Feature pyramid is a strategy for dealing with multi-scale target detection, which could be realized by adding layers of characteristics at various scales to backbone network [33]. Feature pyramid network (FPN) serves to establish connections among different layers of feature maps and perform feature fusion and up-sampling operations to generate pyramid structures with rich semantic information and multi-scale features, helping the network better detect targets of various sizes and scales [34]. The structure of neck module is presented in Fig.3.4.

3.1.3. Head module. In YOLO v5, head module (shown in Fig. 3.5) is responsible for performing target detection task on the last layer of network feature map, which usually consists of multiple convolutional layers for extracting features and generating target detection results [35]. The head module in YOLOv5 applied a series of convolutional operations on the last convolutional layer to generate a bounding box for the target and a corresponding class confidence score. These predictions were applied to determine the presence of targets in the image and their corresponding classes.

3.2. Improvements to initial anchor box. YOLO v5 algorithm inherits the anchor box mechanism of previous generations of YOLO algorithm with the difference that YOLO v5 algorithm innovatively embedded adaptive anchor box mechanism. It significantly enhanced the efficiency of the algorithm [36]. However, the prior frame of YOLO v5 target detection network was based on the COCO dataset obtained by clustering

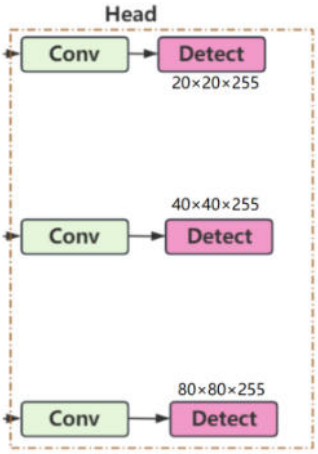

Fig. 3.5: Head module structure.

during training and large target detection in the dataset accounts for more. However, in the current detection scenario, small and medium-sized targets were predominate and were still mainly targeted as pipeline defective targets, which inability to fit well the anchor box acquired on the COCO dataset. The primary drawback of K-means technique is that the amount of clusters-K and the initial cluster centers need to be confirmed by themselves, and an unreasonable number of clusters and cluster centers will make the results uninterpretable. Therefore, this research recommended using K-means++ algorithm to recalculate the anchor boxes used in pipeline defect target identification to improve the accuracy of the algorithm.

3.2.1. K-means. The main principle of K-means algorithm is to first choose K cluster centers at random according to the principle of nearest neighbor to sample points to be classified into each cluster. Then, the center of mass of each cluster is recalculated through averaging method to determine new cluster center. Iterating is continued until the clustering results of all samples no longer change.

K-means clustering algorithm is consisted of the following main steps.

Step 1: Selection of clustering centers. K samples from dataset X are randomly selected as initial clustering centers;

Step 2: Calculation of Euclidean distance. Distances from all sample points to K cluster cores are individually calculated, the closest cluster core to the point is found, and the obtained core is attributed to the corresponding cluster;

Step 3: Updating the clustering center. After assigning all points to K clusters into which the dataset X is divided, the center of gravity (average distance from the center) of each cluster is re-computed and designated to be a new "cluster core".

Step 4: Steps 2 and 3 are repeated until each clustering center no longer changes.

3.2.2. K-means++. The original YOLO v5 algorithm integrated K-means and genetic algorithms in auto anchor, which performed the computation of the anchor value of the data before training was started. Based on the obtained best possible recall (BPR) value, it could be determined whether the dataset needed to recalculate the anchor[37]. K-means clustering algorithm required human intervention in determining the value of K. The result might not be a globally optimum solution, which greatly reduced the overall operating efficiency of the algorithm [38]. Therefore, in this research, it was decided to replace K-means algorithm with K-means++ algorithm to recluster the dataset which was optimized to decrease errors and improve detection algorithm accuracy. K-means++ algorithm is consisted of the following steps:

Step 1: The initial clustering center C1 is chosen at random from dataset X;

Step 2: The shortest distance $d(x)$ between each sample and the already existing clustering center is determined;

Step 3: The probability $P(x)$ hat each sample point would be chosen as the next cluster center is calculated

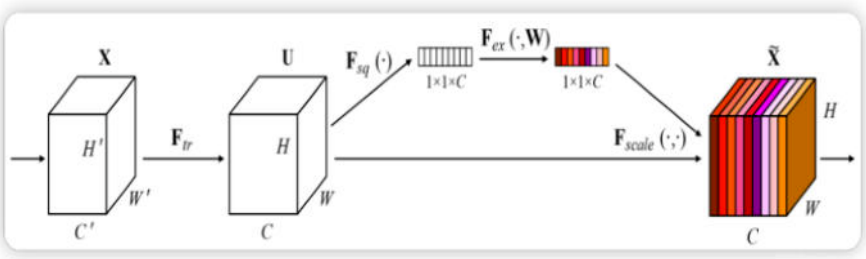

Fig. 3.6: SE module structure.

and then, the sample point with the highest probability value (or probability distribution) is chosen as the next cluster center $P(x)$, as stated in Equation 3.1

$$P(x) = \frac{d(x)^2}{\sum_{x \in X} d(x)^2} \tag{3.1}$$

Step 4: Steps 2 and 3 are repeated until a total of K cluster centers are screened;
Step 5: Calculation of the Euclidean distance. The distances from all sample points to K cluster cores are individually calculated, the closest cluster core to the point is found, and it is attributed to the corresponding cluster;
Step 6: Updating the clustering center. After assigning all points to the K clusters into which the dataset X is divided, the center of gravity (average distance from the center) of each cluster is re-computed and designated as a new "cluster core".
Step 7: Steps 5 and 6 are iterated until each clustering center no longer changes.

3.3. Fusion Attention Module. Due to its high detection speed and accuracy, YOLO v5 is frequently used in target detection and defect recognition applications. However, there is a certain error when detecting unclear features or small targets and images obtained in natural environments may have occlusion. Therefore, in order to address the aforementioned issues, it is required to increase the feature extraction capability of the detected targets. Adding attention mechanism in YOLO v5 is the most common way to enhance its feature extraction ability and despite the fact that it increases the total amount of parameters, it can improve accuracy.

3.3.1. SE module. Squeeze-and-excitation (SE) model is an attentional mechanism to enhance the performance of neural networks. It dynamically learns the importance of features among different channels and improves the network's attention to important features. The main functions of SE module are excitation and squeeze, which are obtained through a series of operations to obtain a weight matrix to reconstruct the original features [39]. The structure of SE algorithm is presented in Fig. 3.6.

3.3.2. CA modules. Channel attention (CA) module is designed to improve the feature representation ability of the network by learning the importance of features among various channels to increase the network's attention to specific features. By introducing CA module, the ability of the neural network to perceive critical features can be effectively improved, which in turn enhances network performance in various visual tasks [40]. The structure of CA algorithm is presented in Fig. 3.7.

3.4. CBAM module. Convolutional block attention module (CBAM) was designed to improve the performance of neural networks by focusing on both channel and spatial information. Channel attention is applied to learn the importance of features among different channels, while spatial attention is employed to learn the correlation among different locations within the feature map, thus allowing the network to focus more on important feature channels and spatial locations[41]. The structure of CBAM algorithm is illustrated in Fig. 3.8.

4. Analysis of experimental results. We allocated training dataset, validation dataset, and test dataset in the ratio of 7:2:1, with a total of 3365 images. The specific quantities are summarized in Table 4.1.

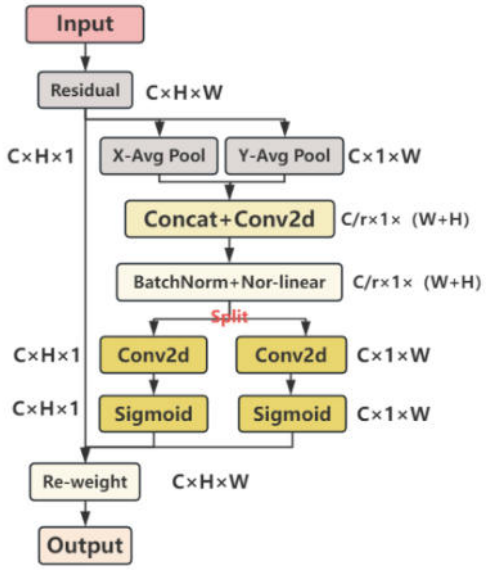

Fig. 3.7: CA module structure.

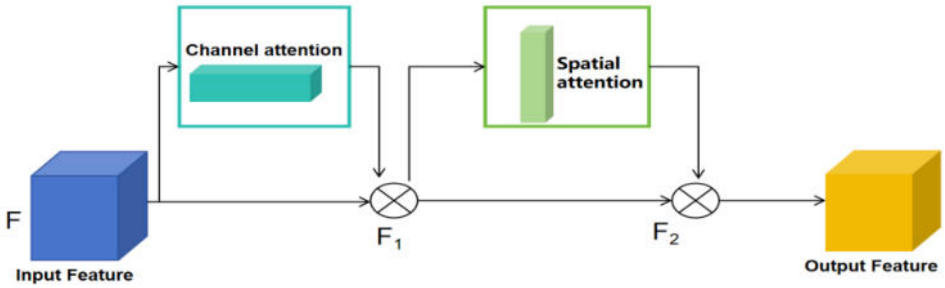

Fig. 3.8: CBAM module structure.

Table 4.1: Specific allocation of data sets.

Defect type	Training	Validation	Test	Total
Cracks	753	227	123	1103
Snap	720	208	110	1038
Holes	822	253	149	1224

4.1. Setting parameters and experimental platform. The working environment is presented in Table 4.2 and the settings of the training parameters are given in Table 4.3.

4.2. Evaluation indicators. The experimental results of this research evaluated the performance of the improved algorithm in terms of mean average precision (mAP), recall, and precision. In target detection, mAP is applied to measure the detection accuracy of the model on multiple categories for evaluating the performance of the overall target detection algorithm where larger mAP values indicated better model performance. The

Table 4.2: Experimental operating environment.

Classification	Versions
Computer operating system	Windows 10 Professional
CPU	i9-9900KF
GPU	NAIDIA GeForce RTX2080Ti 12G
RAM	32G
Python	3.8
Pytorch	1.9
CUDA	11.1

Table 4.3: Experimental training setting.

Name	Image size	learning rate	Epoch	Batch-size
Parameter setting	640×480	0.01	200	16

Table 4.4: Ablation experiments with different image pre-processing procedures.

Greyscale processing	Image enhancements	Filtering and denoising	Edge detection	Threshold segmentation	mAP/%	Time/h
×	×	×	×	×	94.01	23.8
✓	×	×	×	×	94.06	16.9
✓	✓	×	×	×	94.85	16.6
✓	✓	✓	×	×	95.22	16.7
✓	✓	✓	✓	×	95.68	14.8
✓	✓	✓	✓	✓	95.85	14.8

equations for recall, precision, and mAP are expressed below:

$$Precision = \frac{TP}{TP + FP} \tag{4.1}$$

$$Recall = \frac{TP}{TP + FN} \tag{4.2}$$

$$AP = \int_0^1 P(R)dR \tag{4.3}$$

$$mAP = \frac{1}{N}\sum_{i=1}^{N} AP_i \tag{4.4}$$

where TP, FP, and FN stand for true positives, false positives, and false negatives, respectively.

4.3. Comparative experiments and analysis of results. It was seen that training YOLOv5 model using preprocessed defective images improved mAP by 1.84% and training speed by 29% compared to the original algorithm, which showed that preprocessing of pipeline defect images improved the training speed and accuracy of the model.

Table 4.5 shows that the K-means algorithm to K-means++ method was successful in boosting overall algorithm detection precision, with mAP increasing by 0.48%.

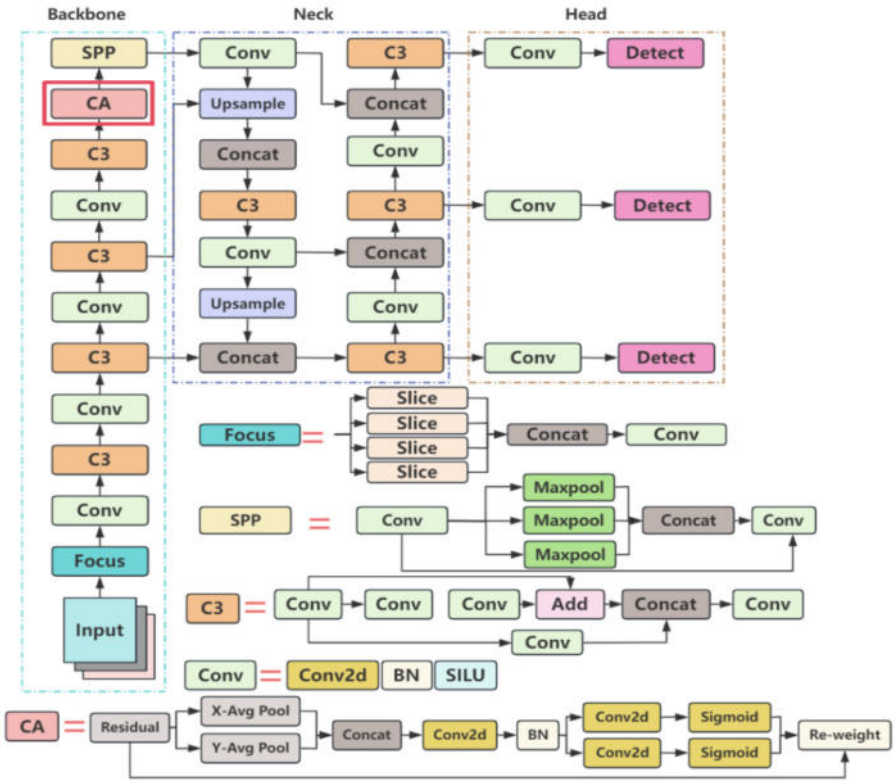

Fig. 4.1: Improved YOLO v5 Structure.

Table 4.5: Comparison of initial anchor box optimisation experiments.

Algorithms	mAP/%	Recall/%	Precision/%	Params/M	Time/h
YOLOv5s	95.85	94.20	94.55	7.06	14.8
YOLOv5s-K++	96.33	94.98	95.26	7.06	14.5

Table 4.6: Comparison of different models of attention mechanisms.

Algorithms	mAP/%	Recall/%	Precision/%	Params/M	Time/h
YOLOv5s	95.85	94.20	94.55	7.06	14.8
YOLOv5s-K++-SE	96.52	97.46	95.97	7.21	15.1
YOLOv5s-K++-CA	97.18	98.06	97.1	7.22	15.4
YOLOv5s-K++-CBAM	95.79	97.73	96.06	7.22	15.6

Comparison of the results of adding different attention mechanism modules is given in Table 4.6 where CA module was found to have the best effect compared with other methods. CA module was added to YOLO v5 model and its structure is shown in Fig.4.1. The trained mAP function curve and loss function curve are illustrated in Fig. 4.2 and confusion matrix is presented in Fig. 4.3. Compared with the original algorithm, the improved YOLO v5 algorithm was better, with 1.33% increase in mAP and 3.83% increase in recall.

To further validate the performance of the improved algorithm, we conducted comparative experiments using two defect detection algorithms of YOLO v7 and YOLO v8. The obtained experimental results are presented in Table 4.7 and Fig. 4.4, with confusion matrix depicted in Fig. 4.5. The experimental results

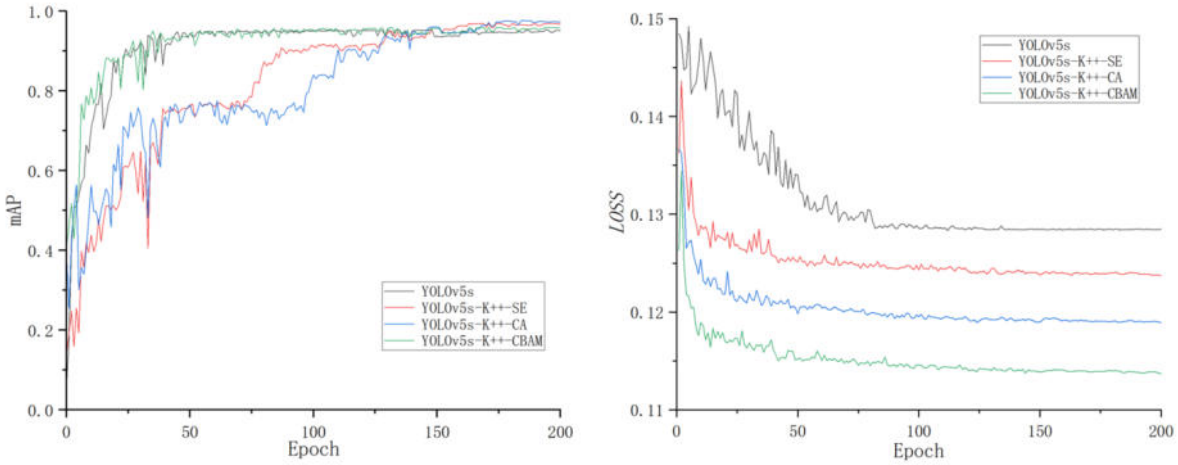

Fig. 4.2: Graph of the mAP and Loss for the different models.

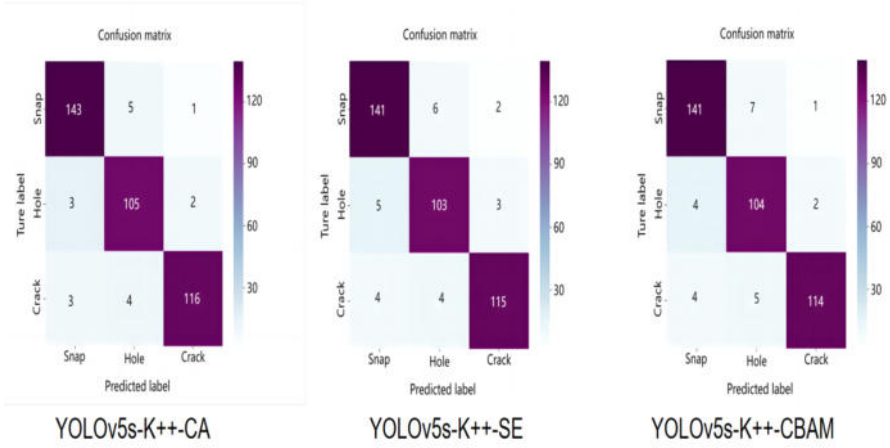

Fig. 4.3: Confusion matrix for different models of attention.

Table 4.7: Comparison of different detection algorithms.

Algorithms	mAP/%	Recall/%	Precision/%	Params/M	Time
YOLOv8	96.75	95.02	95.82	6.86	14.1
YOLOv7	96.29	94.91	95.61	6.95	14.6
YOLOv5s-K++-CA	97.18	98.03	97.1	7.22	15.4

demonstrated that improved YOLO model achieved higher mAP, precision, and recall compared to the remaining two algorithms, where mAP was 0.43% higher than that obtained from YOLO v8 and 0.89% higher than that of YOLO v7. Therefore, it could be inferred that YOLO v5s-K++-CA was an accurate and stable tool for pipeline defect detection. The developed method could be applied to detect pipeline defects and ensure pipeline safety.

Using trained pipeline defect detection model to detect gas pipeline defects, it was found that the improved

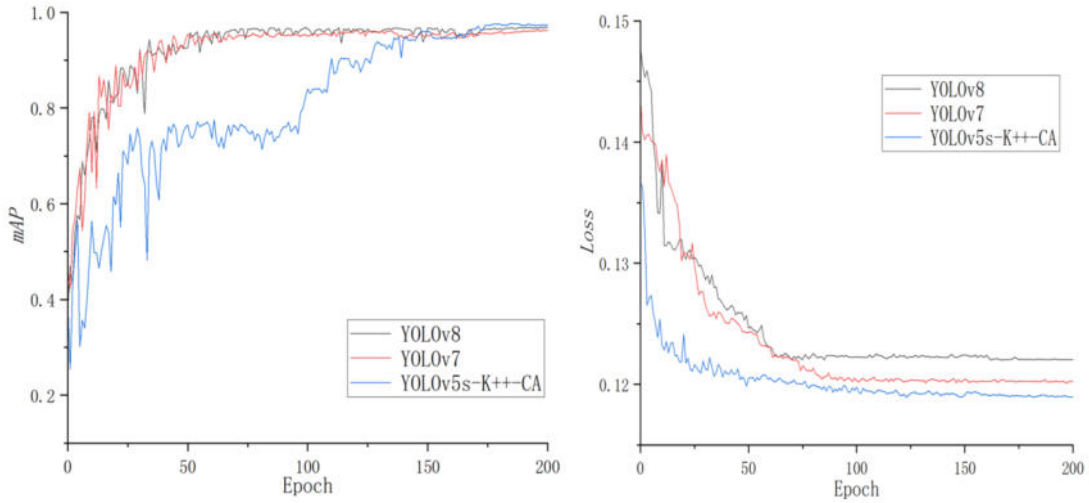

Fig. 4.4: Graph of mAP and Loss for the different detection algorithms .

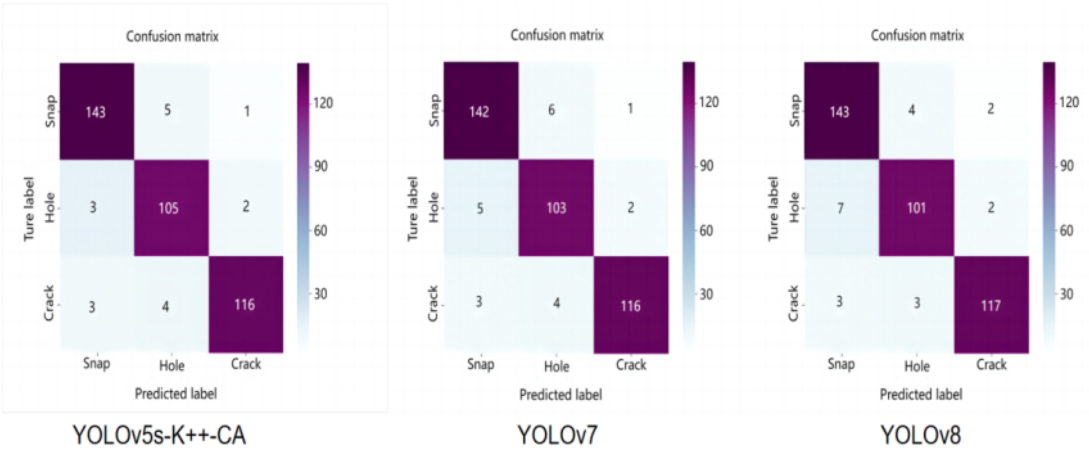

Fig. 4.5: Confusion matrix for different detection algorithms.

algorithm was able to provide much higher detection capability compared to the original algorithm. From Fig. 4.6, it was seen that the updated approach presented a greater confidence level compared to the original algorithm. For the three common defects of cracks, snaps, and holes, the developed method provided higher recognition rates and the maximum confidence was improved by 0.2.

5. Conclusion. To address the challenges of low natural gas pipeline defect detection accuracy and poor stability, we introduced an improved defect detection method based on YOLO v5 algorithm. Experimental results demonstrated that the improved YOLO v5 model exhibited strong robustness and precision in detecting pipeline defects and as a non-destructive testing method, it could be used to detect pipeline defects.

The primary conclusions of this research were as follows:

1. In response to frequent occurrence of varying degrees of leakage and other anomalies in oil and gas pipelines, through experimental simulation of different abnormalities in the pipeline, the data collection and manual marking production of corresponding data set, to lay the groundwork for utilizing target detection methods in studying pipeline leakage and other anomalies in the future.

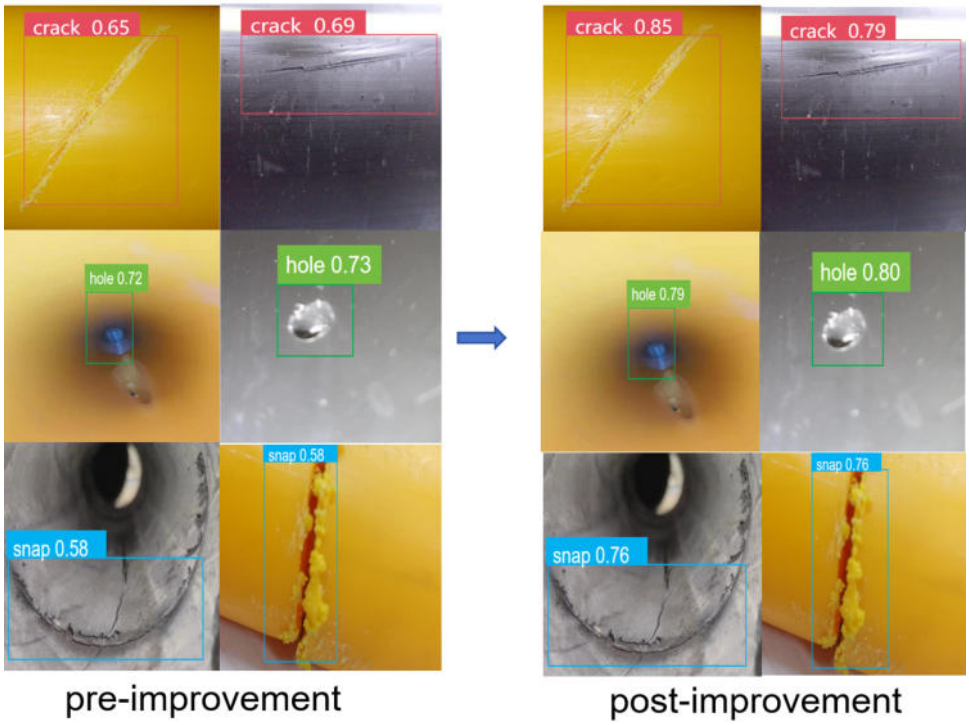

Fig. 4.6: Comparison the effect before and after model improvement.

2. To enhance the quality of pipeline defect images, first, images were in grayscale using weighted average method. Then, the contrast between pipeline background and any defects was enhanced by applying gamma transform. Finally, noise was reduced in images using dual filtering.
3. To simplify the data and enhance the training speed and effectiveness of the model, we utilized improved Sobel algorithm and adaptive thresholding method to detect defective image edges and threshold segmentation to generate binary images. Then the model was trained with binary images to reduce its dependence on color features, making the model more concerned with target shape.
4. In order to enhance the precision and efficiency of pipeline defect detection, YOLOv5's K-Means algorithm was improved and K-Means++ algorithm was employed to determine the initial center of the anchor frame. Introduction of CA attention mechanism enhanced the perceptual ability of the convolutional neural network in target detection, thus improving the accuracy and robustness of the detection process.

In order to achieve better detection results and make the model more practical, the dataset needs to be expanded to include various types and resolutions of pipeline defect images to further improve the ability of real-time pipeline defect monitoring and detection model structure needs to be optimized to make it more universally practical, which are considered as future works to be improved.

REFERENCES

[1] Wang, Y., Feng, G., Lin, N., Lan, H., Li, Q., Yao, D., & Tang, J. (2023), A Review of Degradation and Life Prediction of Polyethylene, The Victor Klee Festschrift, Applied Sciences, 13(5), p.3045.

[2] Martínez-Palou, R., de Lourdes Mosqueira, M., Zapata-Rendón, B., Mar-Juárez, E., Bernal-Huicochea, C., de la Cruz Clavel-López, J., & Aburto, J. (2011),Transportation of heavy and extra-heavy crude oil by pipeline: A review, Journal of petroleum science and engineering,75(3-4), pp.274-282.

[3] Zha, S., Lan, H. Q., & Huang, H. (2022),Review on lifetime predictions of polyethylene pipes: Limitations and trends. International Journal of Pressure Vessels and Piping, 198, p.104663.

[4] Li, P., Wang, F., Gao, J., Lin, D., Gao, J., Lu, J., ... & Liu, C. (2022) ,Failure Mode and the Prevention and Control Technology of Buried PE Pipeline in Service: State of the Art and Perspectives. Advances in Civil Engineering, 2022.
[5] Zha, S., & Lan, H. Q. (2021) Fracture behavior of pre-cracked polyethylene gas pipe under foundation settlement by extended finite element method. International Journal of Pressure Vessels and Piping, 189, p.104270.
[6] Yin, X., Chen, Y., Bouferguene, A., Zaman, H., Al-Hussein, M., & Kurach, L. (2020) A deep learning-based framework for an automated defect detection system for sewer pipes. Automation in construction, 109, p.102967.
[7] Wang, Y., Fu, Q., Lin, N., Lan, H., Zhang, H., & Ergesh, T. (2022) Identification and Classification of Defects in PE Gas Pipelines Based on VGG16. Applied Sciences, 12(22), p.11697.
[8] Han, F., Yao, J., Zhu, H., & Wang, C. (2020) Underwater image processing and object detection based on deep CNN method. Journal of Sensors, 2020.
[9] Dong, S., Sun, X., Xie, S., & Wang, M. (2019) Automatic defect identification technology of digital image of pipeline weld. Natural Gas Industry B, 6(4): pp.399-403.
[10] Wang M, Kumar S S, Cheng J C P. (2021) Automated sewer pipe defect tracking in CCTV videos based on defect detection and metric learning. Automation in Construction, 121: p.103438.
[11] Bondada, V., Pratihar, D. K., & Kumar, C. S. (2018). Detection and quantitative assessment of corrosion on pipelines through image analysis. Procedia Computer Science, 133, pp.804-811.
[12] Myrans, J., Everson, R., & Kapelan, Z. (2019) Automated detection of fault types in CCTV sewer surveys. Journal of Hydroinformatics, 21(1), pp.153-163.
[13] Ye, X., Zuo, J. E., Li, R., Wang, Y., Gan, L., Yu, Z., & Hu, X. (2019) Diagnosis of sewer pipe defects on image recognition of multi-features and support vector machine in a southern Chinese city. Frontiers of Environmental Science & Engineering, 13, pp.1-13.
[14] Fang, X., Guo, W., Li, Q., Zhu, J., Chen, Z., Yu, J., ... & Yang, H. (2020) Sewer pipeline fault identification using anomaly detection algorithms on video sequences. IEEE Access, 8, pp.39574-39586.
[15] Kumar, S. S., Abraham, D. M., Jahanshahi, M. R., Iseley, T., & Starr, J. (2018) Automated defect classification in sewer closed circuit television inspections using deep convolutional neural networks. Automation in Construction, 91, pp.273-283.
[16] Chen, K., Li, H., Li, C., Zhao, X., Wu, S., Duan, Y., & Wang, J. (2022) An Automatic Defect Detection System for Petrochemical Pipeline Based on Cycle-GAN and YOLO v5. Sensors, 22(20), p.7907.
[17] Zhao, X., Wang, X., & Du, Z. (2020, October) Research on detection method for the leakage of underwater pipeline by YOLOv3. In 2020 IEEE international conference on mechatronics and automation (ICMA) (pp. 637-642). IEEE.
[18] Yan, W., Liu, W., Bi, H., Jiang, C., Zhang, Q., Wang, T., ... & Sun, Y. (2023) Yolo-pd: Abnormal signal detection in gas pipelines based on improved yolov7. IEEE Sensors Journal.
[19] Peng, D., Pan, J., Wang, D., & Hu, J. (2022, September) Research on Oil Leakage Detection in Power Plant Oil Depot Pipeline Based on Improved YOLO v5. In 2022 7th International Conference on Power and Renewable Energy (ICPRE) (pp. 683-688). IEEE.
[20] Yin, X., Chen, Y., Bouferguene, A., Zaman, H., Al-Hussein, M., & Kurach, L. (2020) . A deep learning-based framework for an automated defect detection system for sewer pipes. Automation in construction, 109, p.102967.
[21] Yiyang, Z. (2014, December) The design of glass crack detection system based on image preprocessing technology. In 2014 IEEE 7th joint international information technology and artificial intelligence conference (pp. 39-42). IEEE.
[22] Jiang, Y., Liu, Z., Li, Y., Li, J., Lian, Y., Liao, N., ... & Zhao, Z. (2020) A digital grayscale generation equipment for image display standardization. Applied Sciences, 10(7), p.2297.
[23] Qi, Y., Yang, Z., Sun, W., Lou, M., Lian, J., Zhao, W., ... & Ma, Y. (2021) A comprehensive overview of image enhancement techniques. Archives of Computational Methods in Engineering, pp.1-25.
[24] Zhang, L., Li, Y., Wang, P., Wei, W., Xu, S., & Zhang, Y. (2019) A separation Caggregation network for image denoising. Applied Soft Computing, 83, p.105603.
[25] Tian, C., Fei, L., Zheng, W., Xu, Y., Zuo, W., & Lin, C. W. (2020) Deep learning on image denoising: An overview. Neural Networks, 131, pp.251-275.
[26] Li, C., Lan, H. Q., Sun, Y. N., & Wang, J. Q. (2021) Detection algorithm of defects on polyethylene gas pipe using image recognition. International Journal of Pressure Vessels and Piping, 191,p.104381.
[27] Restivo, M. C., Campbell-Washburn, A. E., Kellman, P., Xue, H., Ramasawmy, R., & Hansen, M. S. (2019) A framework for constraining image SNR loss due to MR raw data compression. Magnetic Resonance Materials in Physics, Biology and Medicine, 32, pp.213-225.
[28] Liu, W., & Wang, L. (2022). Quantum image edge detection based on eight-direction Sobel operator for NEQR. Quantum Information Processing, 21(5), p.190.
[29] Liao, J., Wang, Y., Zhu, D., Zou, Y., Zhang, S., & Zhou, H. (2020) Automatic segmentation of crop/background based on luminance partition correction and adaptive threshold. IEEE Access, 8, pp.202611-202622.
[30] Sozzi, M., Cantalamessa, S., Cogato, A., Kayad, A., & Marinello, F. (2022) Automatic bunch detection in white grape varieties using YOLOv3, YOLOv4, and YOLOv5 deep learning algorithms. Agronomy, 12(2), p.319.
[31] Qi, J., Liu, X., Liu, K., Xu, F., Guo, H., Tian, X., ... & Li, Y. (2022) An improved YOLOv5 model based on visual attention mechanism: Application to recognition of tomato virus disease. Computers and electronics in agriculture, 194, p.106780.
[32] Liu, Y., Li, W., Tan, L., Huang, X., Zhang, H., & Jiang, X. (2023) DB-YOLOv5: A UAV Object Detection Model Based on Dual Backbone Network for Security Surveillance. Electronics, 12(15), p.3296.
[33] Chai, E., Ta, L., Ma, Z., & Zhi, M. (2021) ERF-YOLO: A YOLO algorithm compatible with fewer parameters and higher accuracy. Image and Vision Computing, 116,p.104317.

[34] Zhou, L. Y., Wei, D., Ran, Y. B., Liu, C. X., Fu, S. Y., & Ren, Z. Y. (2023) . Reclining Public Chair Behavior Detection Based on Improved YOLOv5. Journal of Advanced Computational Intelligence and Intelligent Informatics, 27(6),pp.1175-1182.
[35] Zhao, C., Shu, X., Yan, X., Zuo, X., & Zhu, F. (2023) RDD-YOLO: A modified YOLO for detection of steel surface defects. Measurement, 214, p.112776.
[36] Gao, M., Du, Y., Yang, Y., & Zhang, J. (2019) Adaptive anchor box mechanism to improve the accuracy in the object detection system. Multimedia Tools and Applications, 78,pp.27383-27402.
[37] Yin, X., Sasaki, Y., Wang, W., & Shimizu, K. (2020) 3D Object Detection Method Based on YOLO and K-Means for Image and Point Clouds. arXiv preprint arXiv:2005.p.02132.
[38] Kapoor, A., & Singhal, A. (2017, February) A comparative study of K-Means, K-Means++ and Fuzzy C-Means clustering algorithms. In 2017 3rd international conference on computational intelligence & communication technology (CICT) (pp. 1-6). IEEE.
[39] Cheng, D., Meng, G., Cheng, G., & Pan, C. (2016) SeNet: Structured edge network for sea Cland segmentation. IEEE Geoscience and Remote Sensing Letters, 14(2), pp.247-251.
[40] Hou, Q., Zhou, D., & Feng, J. (2021) Coordinate attention for efficient mobile network design. In Proceedings of the IEEE/CVF conference on computer vision and pattern recognition (pp. 13713-13722).
[41] Woo, S., Park, J., Lee, J. Y., & Kweon, I. S. (2018) . Cbam: Convolutional block attention module. In Proceedings of the European conference on computer vision (ECCV) (pp. 3-19).

Edited by: Jingsha He
Special issue on: Efficient Scalable Computing based on IoT and Cloud Computing
Received: Mar 4, 2024
Accepted: Apr 5, 2024